Groundwater chemistry patterns in the phreatic aquifer of the central Belgian coastal plain

Alexander Vandenbohede *, Luc Lebbe

Research Unit Groundwater Modelling, Dept. Geology and Soil Science, Ghent University Krijgslaan 281 (S8), B-9000 Gent, Belgium

ARTICLE INFO

ABSTRACT

The Holocene geological evolution of the Belgian coastal plain is dominated by a transgression of the North Sea, silting up of the coastal plain and human intervention (impoldering). This has led to a typical pattern in groundwater quality which is discussed here for the central part of the coastal plain. Therefore, a database with available groundwater samples is composed. Water type according to the Stuyfzand classification is determined and different hydrosomes and their hydrochemical facies are identified. Based on this, the origin and evolution of the water types is explained using Piper plots and geochemical calculations with PHREEQC. Before the impoldering, salinising and freshening conditions alternated with a general salinisation of the aquifer after about 3400 BP. This results in a dominance of brackish and salt NaCl subtypes which are still found in the deeper part of the aquifer. The subsequent impoldering resulted in an major freshening of the aquifer leading to NaHCO$_3$, MgHCO$_3$ and CaHCO$_3$ subtypes. Overall, mixing, cation exchange, carbonate mineral dissolution and oxidation of organic matter are identified as the major processes determining the general water quality. The close link between geological evolution, water quality and what is still observable today is illustrated with this example of the Belgian coastal plain.

© 2011 Elsevier Ltd. All rights reserved.

1. Introduction

Coastal areas often exhibit a complex distribution of freshwater and saltwater, or, in general, of different water types. The origins of this distribution are many and varied (Stuyfzand and Stuurman, 1994; Costudio, 1997; Custodio, 2010; Post et al., 2003): seawater intrusion due to overexploitation, fossil seawater from former inundations, evaporation or dissolution of salt deposits, etc. Stuyfzand and Stuurman (1994) for instance discern 11 sources of salt. Understanding the origin of the fresh–saltwater distribution and its dynamics is a prerequisite for effective management of available water resources (e.g. van Dam, 1999). This paper maps the occurrence of different water types in the Belgian coastal plain and aims to describe the relevant processes accounting for the different geochemical characteristics in relation with Holocene coastal evolution.

Inland encroachment of seawater, due to overexploitation, is an often encountered reason for the occurrence of saltwater (e.g. Calvache and Pulido-Bosch, 1997; Stamatis and Voudouris, 2003; Capaccioni et al., 2005; El Yaouti et al., 2009; Barlow and Reichard, 2010; Custodio, 2010). On the other hand, many coastal areas have a complex fresh–saltwater distribution because of the presence of

fossil saltwater (Jones et al., 1999), for instance as a relic of Holocene transgressions. Such is the case along the North Sea coast: the north of France, Belgium (De Breuck and De Moor, 1972, 1974), the Netherlands (De Vries, 1981; Stuyfzand, 1993a; Post et al., 2003; Stuyfzand and Stuurman, 2008), and Germany (Grube et al., 2000; Wiederhold et al., 2010). Other, similar settings are found in many deltaic areas worldwide with similar hydro(geo)logical conditions (Coleman, 1981; Oude Essink et al., 2010), including the Po, Mississippi, Nile, Mekong, Chinese and Indian deltas and the US Atlantic coast. The chemical composition of groundwater in such coastal aquifers is mainly controlled by conservative mixing of freshwater and seawater and a variety of water–rock interaction processes such as cation-exchange, redox reactions, and carbonate mineral dissolution and precipitation (Jones et al., 1999; Appelo and Postma, 2005; Andersen et al., 2005; Sivan et al., 2005). Beekman (1991) clearly explained the evolution in water quality because of freshening as a combined effect of cation exchange, calcite dissolution, and organic matter degradation and this has been observed and described in many aquifers worldwide (e.g. Stuyfzand, 1993a,b; Pulido-Leboeuf, 2004; Andersen et al., 2005; Sivan et al., 2005; El Yaouti et al., 2009; Rusak and Sivan, 2010). Additionally, historic evolution of water quality can still be seen by studying the patterns of groundwater quality in an aquifer (Stuyfzand, 1999). As will be elaborated in this paper, the Belgian coastal plain offers a good example of how these water qualities can be linked to local geology, Holocene evolution and human intervention.

---

* Corresponding author. Tel.: +32 9 2644652; fax: +32 9 2644653.
E-mail address: alexander.vandenbohede@ugent.be (A. Vandenbohede).

The hydrochemistry of the phreatic aquifer of the Belgian coastal plain is testament of the close link between Holocene geological evolution and water quality as is observed in many coastal areas. The fresh–saltwater distribution is determined by geological evolution after the last Ice Age whereby the Holocene transgression of the North Sea (Baeteman, 1999) resulted in silting up of the coastal plain. The quality of recharge water changed thereby spatially and temporally because of highly dynamic environments (mud flats, saltwater marshes, freshwater marshes) and changing influences of the sea in the area. Late-Holocene human activities such as land reclamation (impoldering) resulted in a final freshening of the aquifer whereby the older brackish and saltwater was replaced by fresh recharge water. With the exception of areas where hydrological boundary conditions have been changed recently (e.g. harbor development, ecological engineering interventions in nature reserves) the fresh–saltwater distribution in the Belgian coastal plain is in equilibrium with the present-day boundary conditions (Vandenbohede et al., 2010). This is in contrast with for instance the neighboring Dutch coastal plain (Oude Essink, 2001; Oude Essink et al., 2010).

The objective of this paper is to determine and describe the different water types, which occur in the Belgian phreatic coastal aquifer. The classification of Stuyfzand (1989, 1993b) will, therefore, be used. Subsequently, the origin and interconnection of these water types is explained and this is related to the Holocene hydrogeologic and geomorphologic evolution of the coastal plain. As such the interaction between this evolution and the fresh–saltwater distribution and its influence on the observed present-day water quality is discussed. The central part of the Belgian coastal plain is chosen because of the amount of available data which has been collected over the last decades.

2. Hydrogeological setting

2.1. Location

The central part of the Belgian coastal plain is located between Nieuwpoort in the south and the seaport of Zeebrugge in the north (Fig. 1). It has a coastline of about 38 km and a width of about 2.5 km. The geology of the coastal plain consists of Quaternary deposits forming the phreatic aquifer, underlain by a substratum of Tertiary age. Fig. 2 shows a west–east cross-section based on hydrogeological mapping of the sediments of the coastal plain (Lebbe et al., 2006). The Quaternary deposits are highly heterogeneous comprising of siliclastic material with varying amounts of shell debris and organic material: dune deposits, clay polder deposits, sandy tidal channel deposits, peat and clay polder deposits, Quaternary cover and, Pleistocene deposits. There is no occurrence of halite, gypsum or dolomite in the deposits. The thickness of the phreatic aquifer increases towards the coast and is a maximum of 45–50 m in the vicinity of Oostende. The Tertiary substratum consists of a succession of aquitards and aquifers (Fig. 2). The Lower-Paniselian and Ypresian aquifer consists of sandy deposits whereas the Paniselian and Ypresian aquitard consists of clays.

2.2. Hydrogeological evolution

Pleistocene sediments consist of fluvial and marine deposits (mainly coarse sand) formed during the Emian interglacial. In the subsequent Weichselian glacial the sea retreated from the area and Emian deposits were partially eroded. Aeolian and fluvial deposits (mainly sandy sediments) remain from this period. During the subsequent Holocene, geological evolution of the study area was determined by transgression of the North Sea and silting up

of the coastal plain (Baeteman, 1985; Baeteman et al., 1999). Before 7500 BP, sea level rose at a rate of about 7 m/ka (Baeteman, 1999). Between 7500 and 5500 BP this rate diminished to about 2.5 m/ka resulting in large parts of the coastal plain being no longer inundated by the sea. A mud-flat environment with mud and salt-marsh deposits developed incised with tidal channels and gullies. A more or less stable coastal barrier was present. During the early part of this geological evolution, the phreatic aquifer was mainly filled with saltwater. From 7500 BP, brackish and freshwater marshes developed which resulted in a partial and mainly shallow freshening of the aquifer. Especially at higher places in the coastal plain, freshwater environments evolved. At some locations, salt marsh vegetation evolved into reed with relict peat accumulations. This was a highly dynamic system with lateral migration of the tidal gullies, salt marshes and freshwater environments. The rate of sea level rise diminished further to about 0.7 m/ka from 5500 BP onwards. This lower rate of sea level rise resulted in an expansion of freshwater marshes and extensive peat layers are a reflection of this. During this period, many parts of the coastal plain were no longer under the constant influence of the sea and only became inundated temporally during major storm events. Renewed invasion of the sea from about 3400 BP ended this period. Probably less sediment supply from within the North Sea was available. Former seaward deposits were eroded and transported inland. The coastline was, therefore, also retreating inland and peat marshes evolved again in a mud-flat environment. Tidal channels drained the peat layers leading to compaction. With this renewed invasion of the sea, seawater could recharge most of the coastal aquifer. This changed finally because of land reclamation (so called impoldering). Dikes around the tidal channels were built probably as early as the 10th century AD, serving to protect the reclaimed land from seawater. A dense network of drainage channels was constructed for this land reclamation. The tidal channels themselves are thought to be reclaimed from the beginning of the 12th century AD onwards (Ervynck et al., 1999). From then on saltwater could recharge the aquifer only during catastrophic flooding events. Under normal conditions, freshwater recharged the aquifer, displacing the older saltwater.

This recent freshening of the aquifer and the replacement of older saltwater resulted in the current fresh–saltwater distribution shown in Fig. 3 which was first mapped by De Breuck et al. (1974) and updated by Vandenbohede et al. (2010). The map shows the depth to the fresh–saltwater interface which is defined as the 1500 mg/L total dissolved solids (TDS) surface. Although this distribution looks very complex, there is a strong correlation with the geology. Freshwater lenses occur at the locations of the old tidal channels. Because of the higher topographic level of these former tidal channels (which evolved to channel ridges) and its permeable (sandy) sediments, the drainage system is less dense. Consequently, freshwater could easily recharge the aquifer, replacing the older saltwater. This was not the case in the adjacent well-drained areas where only a limited amount of freshwater could recharge, the main portion being drained towards the sea. The most distinct example of a freshwater lens is the 'Houtave channel ridge', south of De Haan (Vandenbohede and Lebbe, 2002). A similar example is to be seen in the area between Zeebrugge and Blankenberge and a less deep freshwater lens occurs south of Bredene. Another example is present in the area south of Oostende.

Comparison of previous data (De Breuck et al., 1974) with more recent data has shown that the general fresh–saltwater distribution is in dynamic equilibrium (Vandenbohede et al., 2010) with the current hydrological boundary conditions. In the last 35 a, no major changes are found with the exception of areas where important hydrological interventions have been undertaken such as for harbor infrastructure or ecological engineering interventions. This is in agreement with simulation results which show that
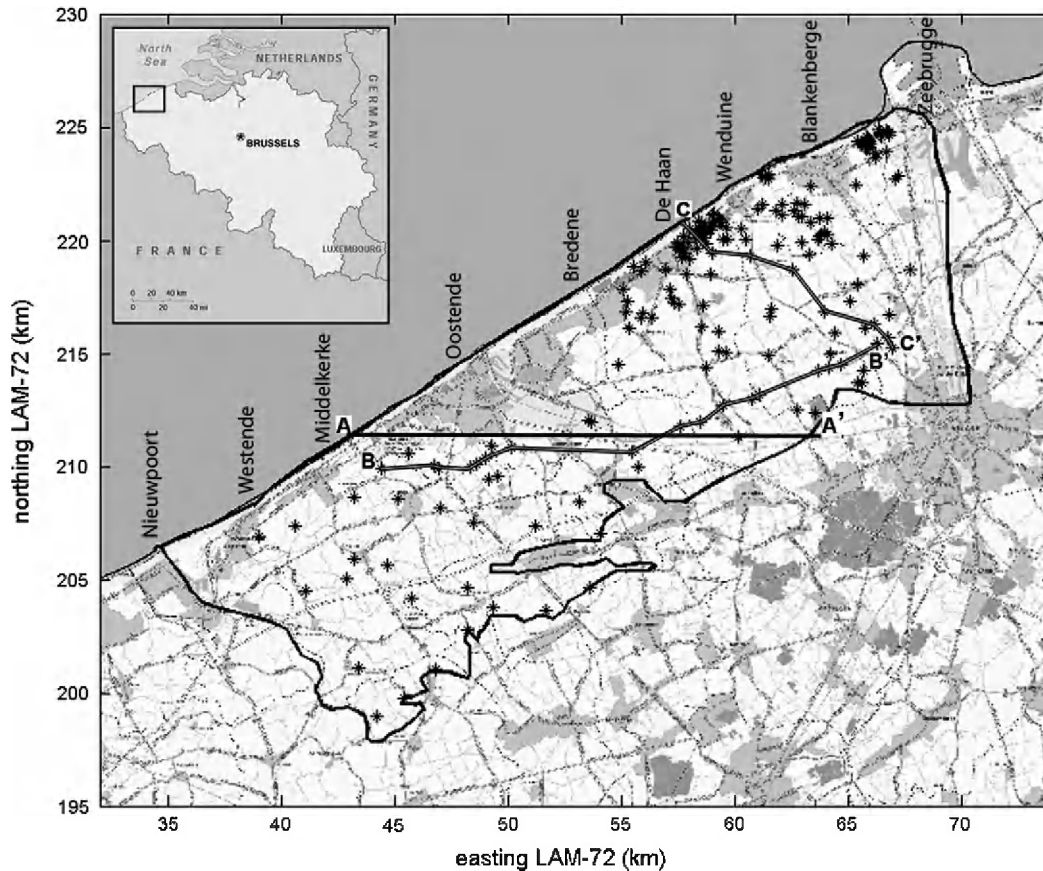
Fig. 1. Localisation of the study area with indication of the sampling locations (*) and cross-sections shown in Figs. 2 and 4. The central coastal plain is located within the black border.
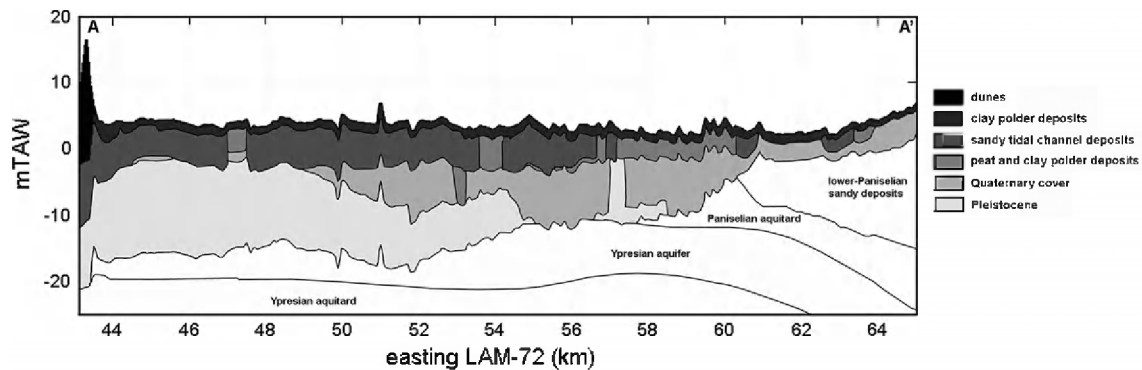

Fig. 2. West–east lithological cross-section through the study area. The location of the cross-section is indicated on Fig. 1. Tertiary substratum is indicated in white. The 0 mTAW forms the Belgian reference level and is 2.36 m below mean sea level.

freshwater lenses reach a dynamic equilibrium within 200–300 a (Vandenbohede and Lebbe, 2002).

3. Materials and methods

3.1. Water quality data

From various sources, a data base with 436 water samples was compiled for this study. These were taken at 193 different locations in the study area (Fig. 1). At most of the locations, screens are present at different depths. Samples of both the deep and shallow parts of the phreatic aquifer are available for most locations. Seventy-four samples were collected for the study of De Breuck et al.

(1974) which resulted in the initial mapping of the fresh–saltwater interface in the coastal plain. Studies and dissertations after 1974 provide a further 244 samples. A number of these studies were done for the Flemish Land Use Agency. The Flemish Environmental Agency manages a phreatic groundwater monitoring network. Groundwater has been sampled twice a year since 2004 at most of the locations of this monitoring network. A mean water composition is calculated for each monitoring point in the case where time series are available, resulting in 106 samples. Finally, 12 samples were recently taken in the framework of the Interreg IVb project, CliWat (Adaptive and sustainable water management and protection of society and nature in an extreme climate), for which the central part of the Belgian coastal plain is a pilot area.
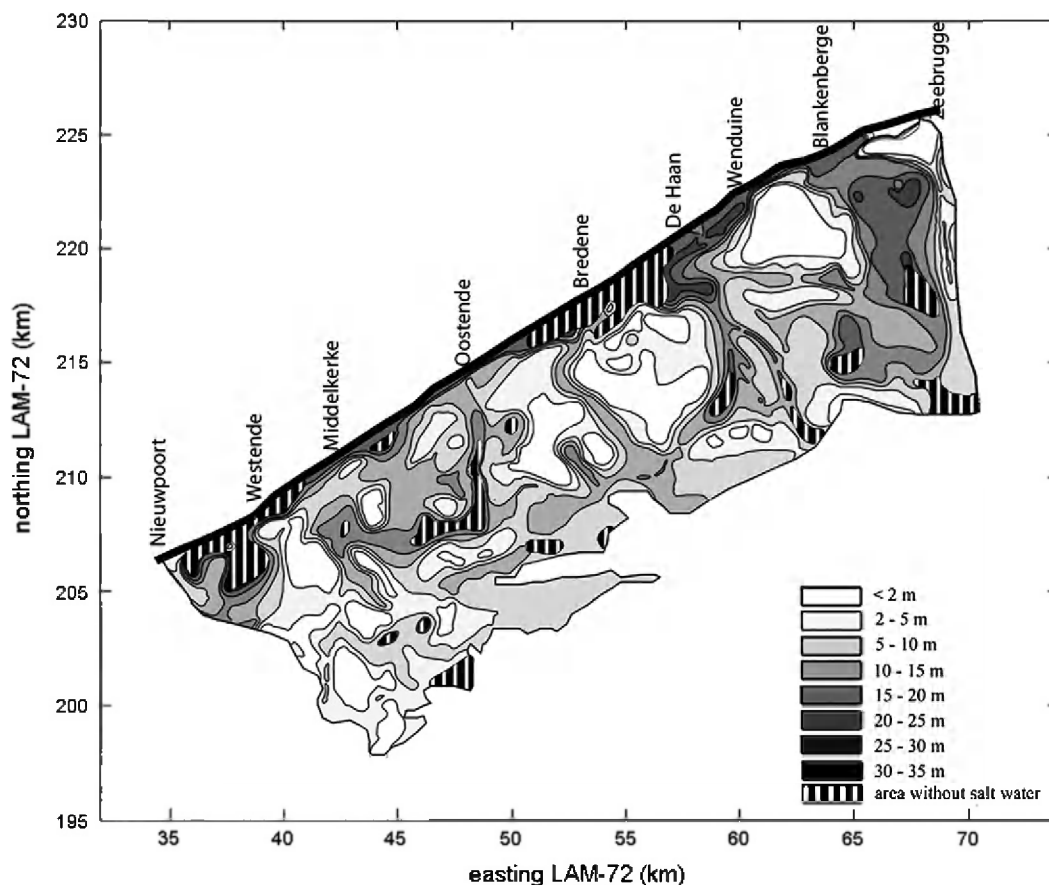
Fig. 3. Depth to the fresh–salt water interface (represented by the 1500 mg/L total dissolved solids isosurface) in the phreatic aquifer of the central Belgian coastal plain as mapped by Vandenbohede et al. (2010).

Because of the large number of data, spread over a large time span, it is difficult to give an overview of the different analytical techniques. Moreover, this is in many cases no longer possible, especially for the older samples. All samples were analysed by accredited laboratories of universities or consultancies, using standard practices. The electrical balance was calculated for each sample before use in this study (Appelo and Postma, 2005). Samples with a difference in electrical balance exceeding 5% were not included.

3.2. Hydrochemical methods

The classification of Stuyfzand (1989, 1991, 1993a) is used to subdivide the water samples in a number of water types. The determination of a water type implies the successive determination of a main type, type, subtype and class of the water sample (Table 1). Each of the four levels of subdivision contributes to the total code (and name) of the water type. Chloride concentration determines the main type of a water sample. Oligohaline (G), oligohaline-fresh (g), fresh (F), fresh-brackish (f), brackish (B), brackish–salt (b), salt (S) and hyperhaline (H) waters are distinguished. Alkalinity, defined by HCO_3^- concentration, determines the type. Alkalinity varies from very low (<31 mg/L HCO_3^-) to extreme alkalinity (>3905 mg/L HCO_3^-). The most important cation and anion determine the subtype. The Stuyfzand classification deviates from common practice where the cation or anion with the highest concentration is chosen. First the dominating hydrochemical family is determined both for cations ($Ca + Mg$, $Na + K + NH_4$ or $Al + H + Fe + Mn$) and anions (Cl, $HCO_3 + CO_3$ or $SO_4 + NO_3 + NO_2$) and then the dominating member of each family is chosen. This methodology results in a possible denomination of otherwise rare

water types like $MgHCO_3$, NH_4HCO_3 or $AlSO_4$. The base exchange index (BEX) defines the class. The BEX can be calculated in different ways. Stuyfzand (2008) evaluated different methods and concluded that for aquifer systems without dolomite, BEX equal to $Na + K + Mg - 1.0716$ Cl (concentrations in meq/L) is the most appropriate, because it not only indicates the right direction (fresh or salt water intrusion), but also the magnitude of the exchange reaction and side reaction with $CaCO_3$. During the calculation, BEX is not only screened on Cl but also on the quality of the hydrochemical analysis (sum cations and sum anions) in order to exclude false positive or false negative values (Table 1). With freshening the class becomes positive due to cation exchange. With salinisation, the reverse is true. The classification of Stuyfzand is well-known for its application in coastal areas for the determination of water types and the evaluation of geochemical processes (e.g. Giménez and Morell, 1997; Stuyfzand, 1999; El Yaouti et al., 2009; Vandenbohede et al., 2009; de Louw et al., 2010; Giménez-Forcada et al., 2010).

Using the water types, hydrosomes and hydrochemical facies are identified. As defined by Stuyfzand (1999), a hydrosome is a 3-dimensional unit of groundwater with a specific origin. Within a given hydrosome, the chemical composition of water varies in time and space due to changes in recharge composition and in flow patterns, and due to chemical processes between the water and the porous medium. These variations are used to subdivide a hydrosome into a number of characteristic zones, called hydrochemical facies, a term introduced by Back (1960). Different hydrosomes and hydrochemical facies are identified by plotting the water types on two cross-sections through the study area. Piper plots are used to show the evolution of various water types into each other. Additionally, Piper plots also help to distinguish graphically between

Table 1
Classification of Stuyfzand (1993a).

Classification	Units	Limits	Code
Main type	Cl (mg/L)	0–5	G – oligohaline
		5–30	g – oligohaline-fresh
		30–150	F – fresh
		150–300	f – fresh-brackish
		300–1000	B – brackish
		1000–10,000	b – brackish-salt
		10,000–20,000	S – salt
		>20,000	H – hyperhaline
Type	HCO_3^- (mg/L)	<31	* – very low
		31–61	0 – low
		61–122	1 – moderately low
		122–244	2 – moderate
		244–488	3 – moderately high
		488–976	4 – high
		976–1953	5 – very high
		1953–3905	6 – rather extreme
		>3905	7 – extreme
Class	BEX^a	$<-(0.5 + 0.02Cl)$	–
		$>-(0.5 + 0.02Cl)$ and $<0.5 + 0.002Cl$ and [b]	0
		$>0.5 + 0.02Cl$	+

[a] $BEX = Na + K + Mg - 1.0716\,Cl$ (meq/L).

[b] $|BEX + \frac{(\sum c - \sum a)}{|\sum c - \sum a|}|(0.5 + 0.02Cl^-) > 1.5|\sum c - \sum a|$ with $\sum c$ and $\sum a$ the sum of cations and anions (meq/L).

different hydrochemical species based on the water types defined by the Stuyfzand classification.

Finally, the aqueous geochemical modeling code PHREEQC (Parkhurst and Appelo, 1999) was used to calculate freshening and salinisation as a column experiment and, evolution of redox zonation. These results are compared with the samples. The freshening and salinization modeling calculates the chemical changes because of the displacement of saltwater by freshwater or vice versa. Therefore, an 8 m long column, subdivided in 40 cells of 0.2 m is considered. Porosity of the sediment column is 0.35 and dispersivity is 0.1 m.

4. Results and discussion

4.1. Water types

In this section, a description is given, using a table and a number of figures, of the different water types, their composition and their occurrence in the study area. Table 2 gives an overview of the different water types, their mean composition and standard deviation. Fig. 4 shows two cross-sections through the study area with an indication of the fresh–saltwater interface as defined in Fig. 3 and the occurrence of different water samples and their classification. Cross-section B–B′ is more or less parallel to the coast and is located in the polder. Cross-section C–C′ is situated perpendicular to the coast and includes the coastal dunes and the polder behind it. Fig. 5 is a Piper plot showing all the water samples indicated according to the subtypes of the Stuyfzand classification. Finally, Fig. 6a and c show the relative percentages of the major ions as a function of Cl⁻ concentration for all water samples. These relative percentages are calculated as the ratio of the concentration of a certain ion (in mmol/L)/ over the sum of all ion concentrations (in mmol/L) in the sample.

Based on the origin of the groundwater, three main hydrosomes can be distinguished: dune hydrosome (DH), polder hydrosome (PH) and the relict Holocene hydrosome (RHH). The RHH comprises the brackish to saltwater which is found below the 1500 mg/L TDS isoline as mapped by De Breuck et al. (1974) and Vandenbohede et al. (2010). Pore water of the RHH originates from before the impoldering. The DH and PH comprise the freshwater above the 1500 mg/L TDS isoline and contain the freshwater which

has replaced the older brackish and saltwater of the RHH. The DH consists of freshwater which recharged in the dunes, whereas the PH contains the freshwater which recharged in the polder. Since both the DH and the PH originate from the displacement of older salt by fresh recharge water, they will be treated together and referred to as DH/PH from here on in this paper. Other tracers (e.g. ^{18}O or trace constituents) are necessary to clearly distinguish between the DH and the PH but are not available. Some smaller hydrosomes exist around major canals which are on a higher level than the polder drainage level (for instance the canal between Brugge and Zeebrugge). Even so, canal bank infiltration can influence some ditches. In that case, freshwater or saltwater which were drained upstream infiltrate and this infiltration water has a different quality than that present in the aquifer. These smaller hydrosomes are excluded here from the discussion since these must be mapped on a much more local and detailed scale. Finally it should be noted that there is no presence of recently intruded intruding North Sea water under the dunes or in the polder. The freshwater lens under the dunes extends to the Tertiary substratum preventing such intrusion of North Sea water.

Table 2 indicates that the number of encountered water types defined by their subtype is somewhat limited: $CaHCO_3$, $MgHCO_3$, $NaHCO_3$, CaCl, CaMix, NaCl, NaMix and $CaSO_4$. Moreover, water types are clearly connected to the hydrosomes and identify different hydrochemical facies. The DH and the PH consist mainly of the $CaHCO_3$ subtype. The $CaHCO_3$ subtype is also the second most occurring (29.5%) in the data set. It consists of oligohaline to fresh-brackish waters and has relatively low TDS. The BEX is in most cases positive or neutral. Only a small percentage of $CaHCO_3$ waters have a negative BEX. The $CaHCO_3$ subtype plots in the vicinity of freshwater in the Piper plot. Calcium-HCO_3 waters consist of 30–60% of HCO_3^- and 10–30% of Ca^{2+} and these are positively correlated. Sodium content comprises between 5% and 30% of the ions and its concentration is strongly positively correlated with the Cl⁻ concentration. A small percentage of the $CaHCO_3$ subtype is brackish. It differs from the fresh $CaHCO_3$ subtype by its low Ca^{2+} (10–15%), high Na^+ (20–25%), high Cl⁻ (20–25%) and low HCO_3^- (25–30%).

The fresh CaMix subtype is also found in the DH and in the PH. It differs from the fresh $CaHCO_3$ subtype because no clearly dominant anion is present due to the slightly higher Cl⁻ (15–30%) and lower

Table 2
Mean composition and its standard deviation for the major ions and cations (mmol/L) and total dissolved solids (TDS, mg/L) for the different water types found in the data set and for sea water and rain water. The percentage (%) gives the relative occurrence of the different water types in the data set.

	%		Na	K	Ca	Mg	Fe	NH₄	Cl	SO₄	NO₃	HCO₃	TDS	pH
(F–f)(3–4)CaHCO₃⁻	1.4	Mean	2.16	0.11	5.57	0.54	0.04	0.24	3.99	0.65	0.02	9.60	1090	7.65
		Stdv	0.61	0.04	4.15	0.35	0.06	0.37	1.29	0.48	0.03	7.27	708	0.43
(g–F–f)(3–4)CaHCO₃⁺	22.0	Mean	2.56	0.48	3.65	1.04	0.02	0.11	2.14	0.85	0.04	8.61	940	7.00
		stdv	1.81	0.72	1.22	0.57	0.03	0.20	1.42	0.63	0.10	2.31	241	0.72
(F–f)(3–4)CaHCO₃0	5.4	Mean	2.15	0.13	4.07	0.51	0.02	0.12	2.91	0.79	0.04	6.96	844	7.15
		Stdv	0.93	0.15	1.69	0.22	0.02	0.19	1.26	0.63	0.28	2.26	274	0.76
B4CaHCO₃⁺	0.7	Mean	7.63	1.01	4.64	0.83	0.05	0.13	8.83	0.36	0.01	10.19	1398	7.46
		Stdv	1.17	0.69	0.43	0.09	0.07	0.02	0.64	0.24	0.02	0.18	20	0.11
(F–f)4MgHCO₃⁺	2.1	Mean	4.13	1.51	2.06	3.14	0.01	0.24	3.03	0.67	0.01	11.77	1210	7.03
		Stdev	2.15	1.06	0.40	0.71	0.01	0.20	1.32	0.51	0.02	2.69	311	0.51
(F–f)(3–4)NaHCO₃⁺	8.0	Mean	9.20	0.76	1.45	0.94	0.03	0.32	4.37	0.34	0.05	10.09	1144	7.21
		Stdev	3.69	0.52	1.08	0.60	0.04	0.30	2.20	0.45	0.10	3.06	323	1.45
B(4–5)NaHCO₃⁺	3.8	Mean	26.19	1.22	1.68	2.03	0.04	0.46	14.26	0.19	0.08	20.29	2557	7.74
		Stdev	8.90	0.38	1.44	1.48	0.06	0.42	5.16	0.30	0.23	5.92	721	0.59
(B–b)(3–5)NaCl⁻	2.8	Mean	79.29	2.86	8.60	11.24	0.09	0.57	105.69	2.86	0.12	14.32	7476	7.12
		Stdv	59.50	1.90	4.07	8.54	0.22	0.64	76.52	3.41	0.29	8.96	4866	0.68
S(3–6)NaCl⁻	12.7	Mean	341.38	7.12	16.28	40.63	0.11	1.08	419.88	11.35	0.12	28.55	27.587	7.10
		Stdv	49.44	1.97	6.68	8.26	0.12	0.81	60.87	6.69	0.14	12.67	3677	0.32
(B–b)(3–6)NaCl⁺	16.4	Mean	87.37	2.51	3.87	9.07	0.04	0.88	89.20	2.06	0.04	22.29	7234	7.38
		Stdv	70.46	1.52	3.09	8.53	0.05	1.13	79.29	3.46	0.04	13.21	5497	0.68
S(3–6)NaCl⁺	4.7	Mean	323.76	6.85	9.12	37.91	0.10	1.16	365.72	13.05	0.14	28.02	25.048	7.13
		Stdv	49.46	1.11	2.98	8.16	0.11	1.26	61.36	8.42	0.20	17.63	3828	0.30
b(2–5)NaCl0	3.5	Mean	101.81	3.02	7.05	10.41	0.03	0.41	118.06	4.89	0.07	12.12	8408	7.48
		Stdv	73.31	1.91	4.33	8.46	0.04	0.38	86.56	5.22	0.09	8.04	5758	0.52
S(2–6)NaCl0	5.9	Mean	344.85	7.78	12.40	42.32	0.14	1.18	408.50	15.38	0.15	24.59	27.329	7.12
		Stdv	63.16	1.25	3.60	8.93	0.15	1.36	74.54	9.67	0.19	16.27	4856	0.22
(B–b)(3–5)CaCl	2.8	Mean	12.21	1.32	6.34	2.01	0.03	0.17	22.20	1.73	0.13	8.02	2095	7.55
		Stdev	5.93	1.79	2.86	1.06	0.06	0.17	12.61	0.93	0.26	3.65	860	0.53
(F–f)(2–4)CaMix	4.3	Mean	3.57	0.49	4.21	0.83	0.06	0.19	4.82	1.64	0.00	6.07	1000	7.54
		Stdev	2.06	0.16	2.06	0.39	0.07	0.26	1.99	1.05	0.00	3.04	453	0.66
(B–b)(3–4)CaMix⁺	0.7	Mean	18.43	0.45	6.86	3.69	0.09	0.11	18.46	5.52	0.01	9.57	2586	6.64
		Stdev	15.24	0.20	3.01	3.76	0.07	0.10	15.06	7.91	0.00	2.19	1763	0.51
(F–f)4CaSO₄⁺	0.5	Mean	5.06	1.05	10.27	1.64	0.08	0.05	3.86	7.76	0.02	10.73	2156	7.40
		Stdv	1.57	0.96	0.07	0.32	0.04	0.03	1.64	0.38	0.02	0.64	128	0.06
(F–b)(2–5)NaMix⁺	2.3	Mean	14.961	0.936	3.646	2.764	0.035	0.349	13.182	3.271	0.033	9.717	1984	7.53
		Stdv	13.266	0.727	3.549	2.701	0.038	0.545	12.981	4.118	0.036	5.706	16.72	0.95
Rainwater			0.12	0.01	0.08	0.02	0.00	0.00	0.27	0.07	0.00	0.00	23.12	7.40
Sea water			406.00	8.50	8.75	50.00	0.00	0.06	474	24.5	0.00	2.6	30.550	7.60

low HCO_3^- (20–35%). The brackish CaMix subtype is very similar to brackish $CaHCO_3$ subtype but with slightly higher Cl^- (25–30%) resulting in the mix designation. The brackish CaMix and $CaHCO_3$ subtypes are mainly found in the transition zone between the DH/PH and the RHH or in the RHH. Also found in the lower part of the freshwater lenses or in the transition between the DH/PH and the RHH are the $NaHCO_3$ and $MgHCO_3$ subtypes. The $NaHCO_3$ is thereby the third most appearing subtype (11.8%) in the data set. It consist of fresh to brackish water samples and contains higher Na^+ (30–45%) than both seawater and freshwater. The only difference between fresh and brackish $NaHCO_3$ subtypes is the higher Cl^- and lower Ca^{2+} of the latter. The NaMix subtype is quite similar to the brackish $NaHCO_3$ only with significantly lower HCO_3^- (15–30%). The $MgHCO_3$ subtype is characterized by relatively high Mg^{2+} (10–15%) and low Ca^{2+} (5–12%). A few samples are of the $CaSO_4$ subtype, characterized by relatively high SO_4^{2-}, and these are all found in the DH/PH. The CaCl subtype is situated between $CaHCO_3$ and the $NaHCO_3$ and $MgHCO_3$ subtypes but with a relatively higher Cl^- concentration.

The NaCl is the most abundant subtype found in the RHH. It is also the most encountered (46%) subtype in the data set and consists of both brackish and saltwater. It plots close to seawater

in the Piper plot. Salt NaCl subtypes have a similar composition (absolute as well as relative concentrations) as seawater. They are determined by high Na^+ (37–41%) and high Cl^- (46–50%). The Ca^{2+} and HCO_3^- concentrations are low but are higher than for pure seawater. Brackish NaCl subtypes have lower Na^+ (30–50%) and Cl^- (30–50%) and this is positively correlated with Cl^-. The Ca^{2+} and HCO_3^- are increased with respect to the salt subtype and seawater.

Fig. 6a and c illustrate that the relative percentages of the major ions correlate with the Cl^- concentration. For high Cl^- (<200 mmol/L) these percentages are almost equal to those of seawater. With decreasing Cl^- the Cl^- percentage decreases, as do the Na^+ percentages. This is in favor of HCO_3^- and to a lesser extent, of Ca^{2+}. Note that Na^+ can have a wide range of values for a given Cl^- concentration which is less so for other ions. For Cl^- less than 10 mmol/L, Ca^{2+} percentage increases significantly, becoming the dominant cation. Also, the Mg^{2+} and the SO_4^{2-} percentages increase.

4.2. DH and PH: cation exchange

The fresh water in the dunes and polders originates from rain water, equilibrated with partial CO_2 pressure in the soil and
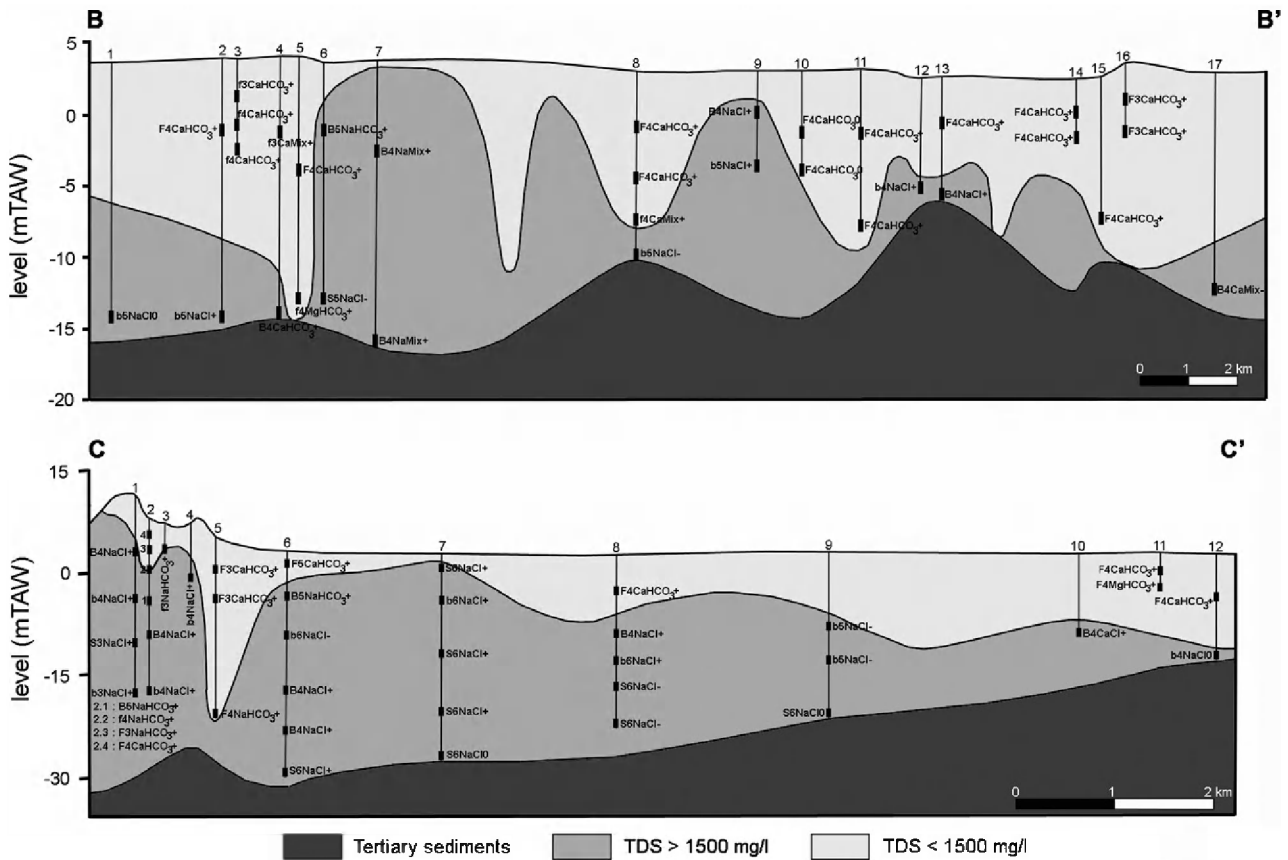
Fig. 4. Two cross-sections through the study area (locations are indicated in Fig. 1), showing the depth of the Tertiary base of the phreatic aquifer, the depth of the fresh–salt water interface (1500 mg/L total dissolved solids) and the sampling locations with indication of the water type.
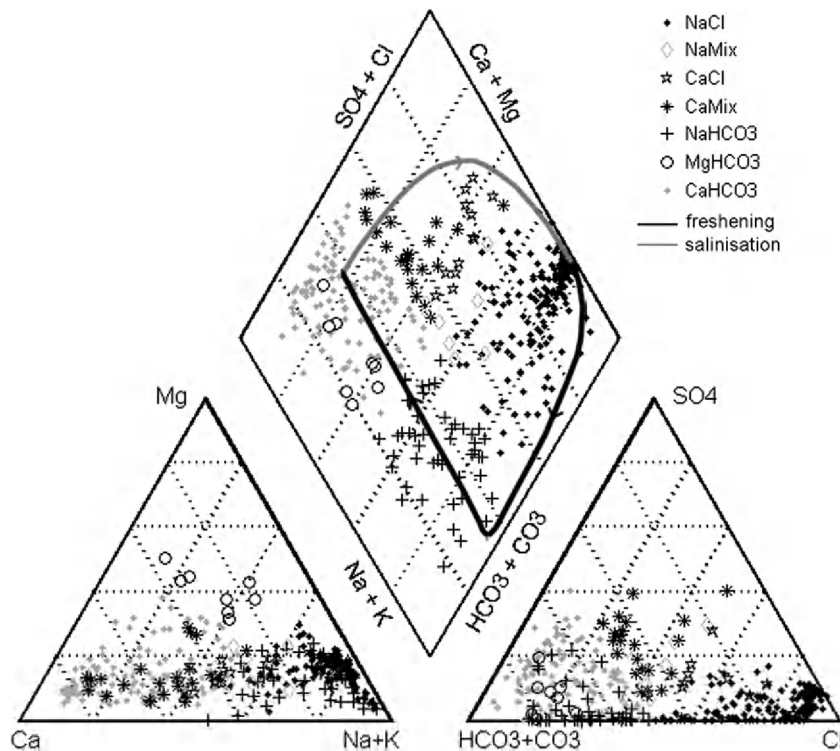

Fig. 5. Piper plot showing all the water samples from the data set grouped according to their subtype in the Stuyfzand classification. The chemical evolution of salt water displaced by freshwater (freshening) or vice versa (salinisation) as calculated with PHREEQC is indicated.
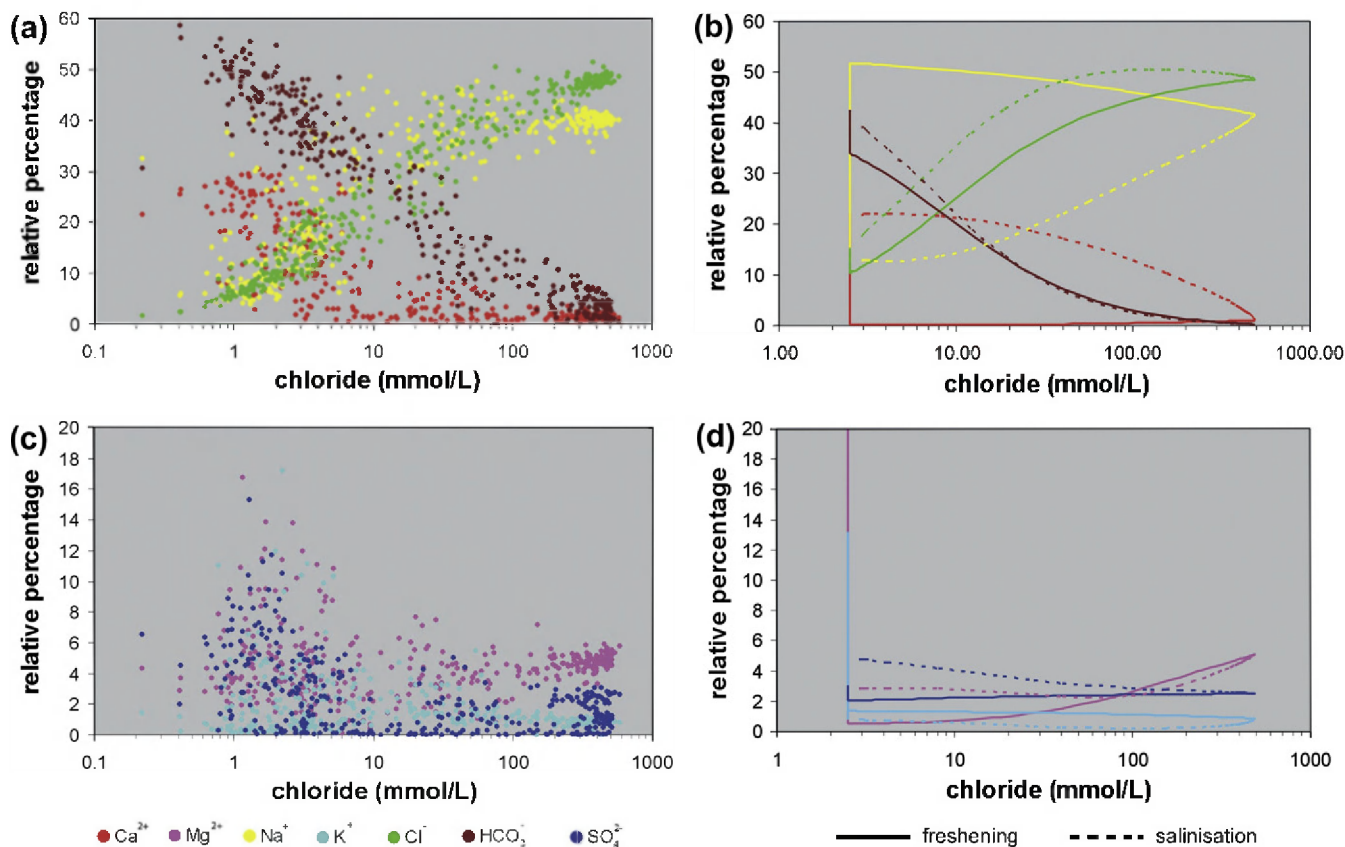
Fig. 6. Relative percentage of the major anions and cations as a function of the Cl⁻ concentration. (a and c) show this for the data set whereas (b and d) show this for the freshening and salinisation experiment as calculated with PHREEQC.

dissolution of carbonate minerals (in an open or closed system). Apart from mixing whereby a transition zone develops between the saline water and the replacing freshwater, cation exchange is one of the major processes. Upon freshwater intrusion, Ca^{2+} expels the previously adsorbed marine cations Na^+, K^+ and Mg^{2+} from the exchanger according to the reaction (Stuyfzand, 1989, 1993a,b):

$$aCa^{2+} + [bNa, cK, dMg]exchanger \iff [aCa]exchanger + bNa^+$$
$$+ cK^+ + dMg^{2+}$$
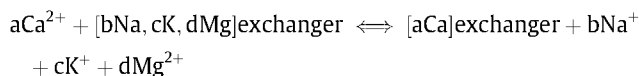
This gives rise to a subsequent series of subtypes: from the NaCl subtype of the saltwater, over $NaHCO_3$ and $MgHCO_3$ to $CaHCO_3$ in the fresh displacement water (Appelo and Postma, 2005). As discussed in the previous section, these subtypes are found in the DH and PH and can be regarded as successive hydrochemical facies within these hydrosomes. Consequently, cation exchange is a determining factor for groundwater composition and evolution. The importance of cation exchange is further illustrated by the BEX.

Fig. 7a–c shows Na^+, K^+ and Mg^{2+} as function of Ca^{2+} for the $CaHCO_3$, $MgHCO_3$ and $NaHCO_3$ subtypes. The $NaHCO_3$ are characterized by high concentrations of Na^+ (up to 45 mmol/L) and Mg^{2+} (up to 5 mmol/L), low concentrations of Ca^{2+} (less than 4 mmol/L) and moderately high concentrations of K^+ (between 0.2 and 2 mmol/L) in comparison with the other subtypes. It represents the first stage of cation exchange whereby Ca^{2+} in the recharge water is exchanged for Na^+ and Mg^{2+}. The $MgHCO_3$ main water type is characterized by high concentrations of Mg^{2+} (between 2.3 and 4.4 mmol/L) and moderate Ca^{2+} concentrations (between 1.5 and 2.8 mmol/L). This is a further stage of cation exchange whereby Ca^{2+} from the recharge water is exchanged mainly by Mg^{2+} from the exchanger. The Na^{2+} concentrations (less than 8 mmol/L) are much lower than in the case

of the $NaHCO_3$ water type. The BEX is positive for both the $NaHCO_3$ and $MgHCO_3$ subtypes clearly indicating the freshening of the aquifer. The $CaHCO_3$ main water type shows a wide range of Ca^{2+} concentrations (1–7 mmol/L) and in general small Na^+ (<5 mmol/L), K^+ (<1 mmol/L) and Mg^{2+} (<1.5 mmol/L) concentrations. Most samples have a positive or neutral BEX, the latter indicating that the sediments are sufficiently flushed with recharge water so that a constant composition is reached. At locations where $CaHCO_3$ samples with both positive and neutral BEX are found, the latter samples occur at more shallower depths than the former.

Cation exchange was modeled using PHREEQC and compared with observed concentrations. The sediment column used for the calculation is initially filled with North Sea water, its composition is given in Table 2. This is displaced by freshwater for which the composition of the $CaHCO_3$0 type is used (Table 2). A cation exchange capacity (CEC) of 6 meq/kg is used which is a typical value for sandy Quaternary deposits (Stuyfzand, 1993b, 1999). Finally, pore water is equilibrated with calcite. The result of this calculation is given in Fig. 8a. It gives the Ca^{2+}, Mg^{2+}, Na^+, K^+ and HCO_3^- concentration as a function of pore volumes of water which is flushed from the sediment column. When the sediments are flushed once, breakthrough of the freshwater is observed and concentrations decrease. Sodium is the dominant cation, resulting in the $NaCl^+$, $NaMix^+$ and finally $NaHCO_3^+$ subtypes. For this latter subtype, Ca^{2+}, Mg^{2+} and K^+ concentrations are, respectively, 0.03, 0.13 and 0.34 mmol/L, which correspond very well with the range observed in the data set. When sediments are flushed 2.15 times Ca^{2+} and Mg^{2+} concentrations again increase slightly resulting in the $MgHCO_3$ main water type. Magnesium becomes 2.25 mmol/L which falls in the observed range. The freshening calculated with PHREEQC is also plotted on the Piper plot (Fig. 5). It illustrates
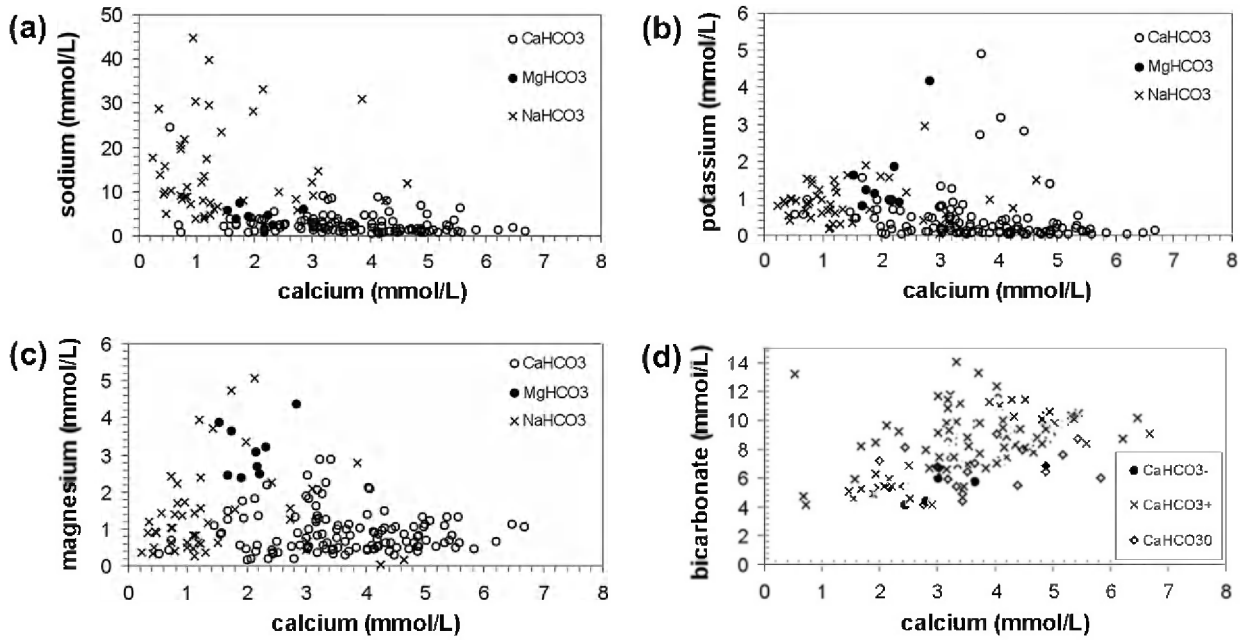
Fig. 7. Chemical composition of the PH and DH: concentrations of Na$^+$, K$^+$ and Mg^{2+} as function of Ca^{2+} for the CaHCO$_3$, MgHCO$_3$ and NaHCO$_3$ subtypes of the dune and polder hydrosome (a–c) and Ca^{2+} versus HCO$_3^-$ for the CaHCO$_3$ subtype (d).
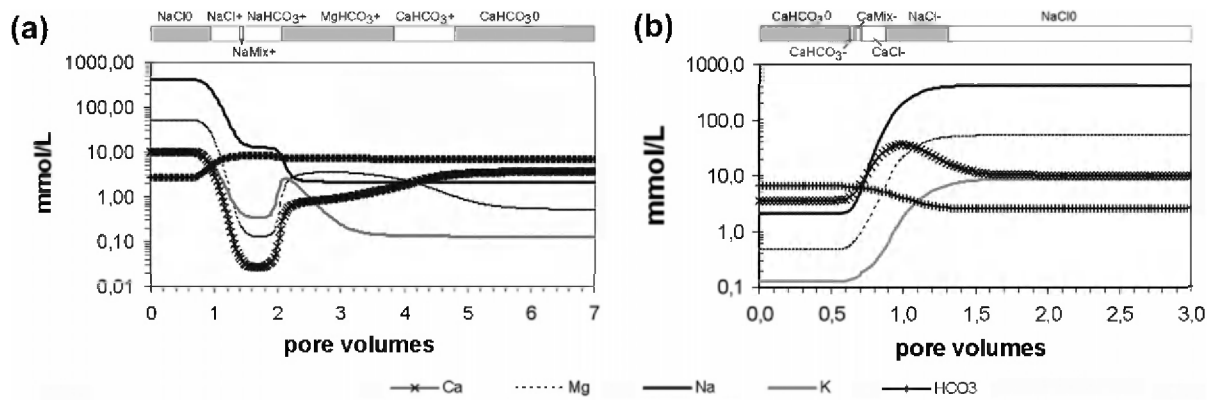

Fig. 8. Evolution of Ca^{2+}, Mg^{2+}, Na$^+$, K$^+$ and HCO$_3^-$ as calculated with PHREEQC for the freshening (a) and salinisation (b) experiment. The abscissa is expressed as the amount of pore volumes of water by which the sediment column is flushed. The resulting water types are given above each figure.

the evolution from the NaCl seawater towards the NaHCO$_3$ subtype and finally towards the CaHCO$_3$ subtype and the origin of the different hydrochemical facies the subtypes represent. On a Piper plot, the evolution of the different subtypes into one another is also very well illustrated. Although it is very hard to distinguish between the MgHCO$_3$ and CaHCO$_3$ subtypes because changes in Ca^{2+} and Mg^{2+} compared to the other ions are relatively small. Relative percentages calculated for the freshening modeling (Fig. 6b and d) compare very well with the observations. Note, however, that the percentage of Na$^+$ should increase during the freshening, until the last stage where it decreases due to the fact that Ca^{2+} becomes the dominant cation. A number of samples indeed show this increasing trend, although a number of other samples show a decreasing trend. This will be discussed further later in the paper.

The NaMix$^+$ subtype is also found in the PH/DH and is the result of cation exchange as indicated by Fig. 8a. It is a transition subtype between the NaCl and the NaHCO$_3$ subtype whereby there is no clear domination of either Cl$^-$ or HCO$_3^-$ hence the Mix designation. Like the NaHCO$_3$ subtype it has low Ca^{2+} (between 1 and 2.5 mmol/

L), very low K$^+$ (between 0.3 and 0.6 mmol/L) and Mg^{2+} (between 0.6 and 0.9 mmol/L), making Na$^+$ the dominant cation with concentrations between 2.5 and 6 mmol/L. Finally, the fresh CaHCO$_3$ subtype with a negative BEX is found in the PH/DH. As the salinisation modeling shows (Fig. 8b), this is the first change pore water undergoes by displacement of CaHCO$_3$0 with saltwater. The negative BEX indicates salinisation which is most probably due to small shifts in the fresh–saltwater interface because of recent changes in hydraulic boundary conditions (for instance drainage levels, levels in canals, influence of infrastructure etc.).

4.3. DH and PH: calcite dissolution and redox sequence

Fig. 7d shows Ca^{2+} versus HCO$_3^-$ concentration for the CaHCO$_3$ subtypes in the data set. These represent the final stage of cation exchange and it is the water type which is most abundant in the DH and PH. Calcium concentrations range from 1 to 7 mmol/L whereas HCO$_3^-$ concentrations range from 3 to 13 mmol/l. There is no clear trend for samples with a positive or a neutral BEX. The few samples with a negative BEX in general show the lowest

HCO_3^- concentrations but this could be due to the limited number of examples. At locations where samples with a positive or a neutral BEX are found, the latter occur at shallower depths. This is in agreement with the final stage of cation exchange whereby the pore water is in equilibrium with the composition of the exchanger. This indicates that the shallow sediments are sufficiently flushed with recharge water to reach equilibrium with the exchanger. The composition of this $CaHCO_30$ water was calculated with PHREEQC and compared with the observed concentrations. Therefore, rain water (Table 2) was equilibrated with a partial CO_2 pressure of 10^{-2} atm and with calcite dissolution (SI = 0). The result is a Ca^{2+} concentration of 1.94 mmol/L and a HCO_3^- of 3.95 mmol/L considering an open system or Ca^{2+} concentration of 4.48 mmol/L and HCO_3^- of 7.21 mmol/L considering a closed system. This compares with the observed concentrations indicating that these two processes indeed determine the composition of the fresh recharge water. Finally, saturation indexes (SI) of the $CaHCO_3$ subtypes were calculated with PHREEQC. These are all between −0.5 and 0.6. Taking into account analytical errors and the fact that minerals in nature are never pure, Stuyfzand (1993a) indicates that equilibrium can be assumed between a SI of −1.0 to 0.3. A SI larger than 0.3 means supersaturation. In that respect all samples are in equilibrium with the calcite phase or slightly supersaturated.

For dune sediments in the northern part of The Netherlands, Stuyfzand (1993b, 1999) found that the upper part of the aquifer consists of decalcified sediments whereby Ca^{2+} concentrations are subsequently lower than deeper in the aquifer. Ampe (1999) found that decalcification depths in the Belgian dune systems are very shallow, except for an old dune system, which is outside the study area. Even so, the decalcification is very limited (maximum 1 m) in the polder (De Leenheer and Van Ruymbeke, 1960). Determination of the carbonate content of Quaternary sediments indeed points to relatively large concentrations. Franceschi (1975) and Devos (1984) reported, for instance, a mean carbonate content of between 2 and 8 wt.%. However, this wt.% can be as high as 25 in horizons with accumulation of shell debris. Subsequently, there is no clear trend of increasing Ca^{2+} concentrations deeper in the aquifer as was reported by Stuyfzand (1993b, 1999) for Dutch sediments.

Bicarbonate concentrations are increased by denitrification, Mn reduction, Fe reduction and SO_4 reduction, combined with the oxidation of organic matter. This gives rise to the redox zonation found along a streamline (e.g. Appelo and Postma, 2005). Recharge water contains dissolved O_2 and this is at first instance used for the oxidation of organic matter. Secondly, NO_3^- is reduced, followed by the reduction of Fe-oxides leading to an increase of the Fe^{2+} concentration. Subsequently, SO_4^{2-} is reduced and the precipitation of Fe sulfide causes a decrease in the Fe^{2+} concentration. Finally, CH_4 appears in the groundwater. Only a few reliable dissolved O_2 measurements exist in the data set. Besides a few exceptions all water samples contain NO_3^- concentrations which are less than 0.8 mmol/L (European Union drinking water limit). Mean NO_3^- concentration of all samples is 0.08 mmol/L with a standard deviation of 0.15 mmol/L. Quaternary sediments in the study area contain a relatively high amount of organic matter. The mean value is between 0.1 and 0.5 wt.% in sandy sediments and this can increase to several wt.% in clay layers (Franceschi, 1975; Devos, 1984). Obviously, this is significantly higher in peat horizons which occur frequently in the sand or clay layers. Consequently, NO_3^- is readily reduced, restricting the NO_3^- concentrations in the groundwater. Fig. 9a shows the SO_4^{2-} concentrations as a function of depth for the $CaHCO_3$, $MgHCO_3$ and $NaHCO_3$ subtypes. In general, SO_4^{2-} concentrations can be as high as 2 mmol/L in the first 5 m. Sulfate concentrations, in general, become less than 0.2 mmol/L deeper in the aquifer, illustrating the reduction of the SO_4^{2-}. Sulfate concentrations are enriched in the upper part of the aquifer mainly
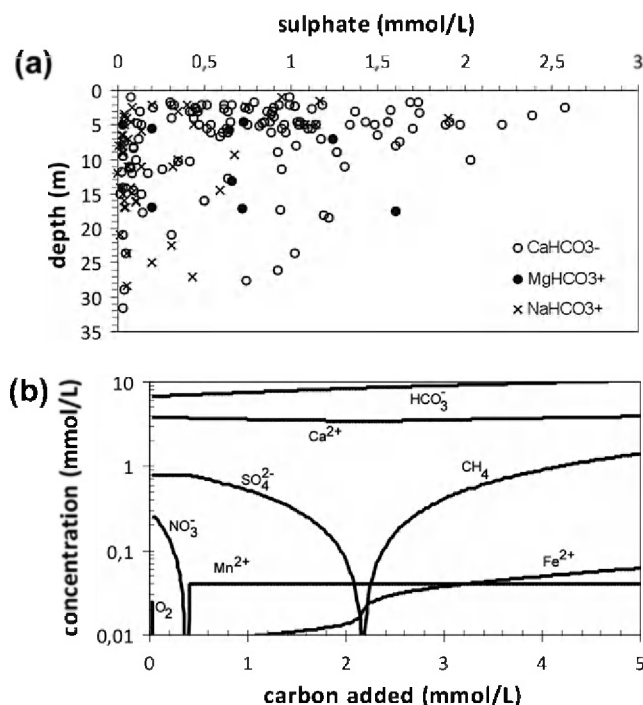

Fig. 9. SO_4^{2-} concentration versus depth for the $CaHCO_3$, $MgHCO_3$ and $NaHCO_3$ main water type (a) and O_2, NO_3^-, SO_4^{2-}, Mn^{2+}, Fe^{2+}, HCO_3^-, Ca^{2+} and CH_4 versus C added as calculated with PHREEQC (b).

by oxidation of pyrite, which is present in the polder sediments. This can result in relative percentages as high as 12% of the total composition (Fig. 6c). Because of the high SO_4^{2-} concentrations, a few samples are of the $CaSO_4$ subtype. This defines a hydrochemical facies which is characterized by relatively high SO_4^{2-} concentrations which can have two origins. It can be due to the already mentioned pyrite oxidation or secondly (and most likely for the high concentrations) by agricultural pollution. The $CaSO_4$ subtype is exclusively found in shallow wells.

Fig. 9b illustrates this redox zonation with a PHREEQC calculation. Water quality of the $CaHCO_30$ water type is used but with a NO_3^- concentration of 0.25 mmol/L and 10 mg/l dissolved O_2. Organic C is added stepwise and the solution is equilibrated with calcite dissolution. Goethite and pyrolusite are sources of Fe and Mn, respectively. Pyrite is allowed to precipitate. Fig. 9b shows that O_2 and NO_3^- are reduced after the addition of 0.3 mmol/L C. With the relatively high amounts of organic material present in the Quaternary sediments, this explains the low NO_3^- concentrations in most of the samples. Sulfate concentrations become very low after the addition of 2.1 mmol/L C. Due to the oxidation of organic matter, HCO_3^- concentrations increase.

4.4. Relict Holocene hydrosome

Subtypes encountered in the RHH are mainly NaCl waters but occasionally, the CaCl subtype is found. A minority of samples classify as CaMix or NaMix. The discussion here will focus on the NaCl subtype. Its Cl^- concentrations are varied ranging from brackish to saltwater (B, b and S main types). The HCO_3^- concentration varies greatly ranging from type 2 to type 6. This results in changing relative percentages of the major ions as a function of the Cl^- concentration as discussed before (Fig. 6a and b). BEX can be positive, negative or neutral. Fig. 10 shows the Na^+, K^+, Ca^{2+}, Mg^{2+}, SO_4^{2-} and HCO_3^- concentrations versus the Cl^- concentration for the NaCl subtype. The concentrations of the different species
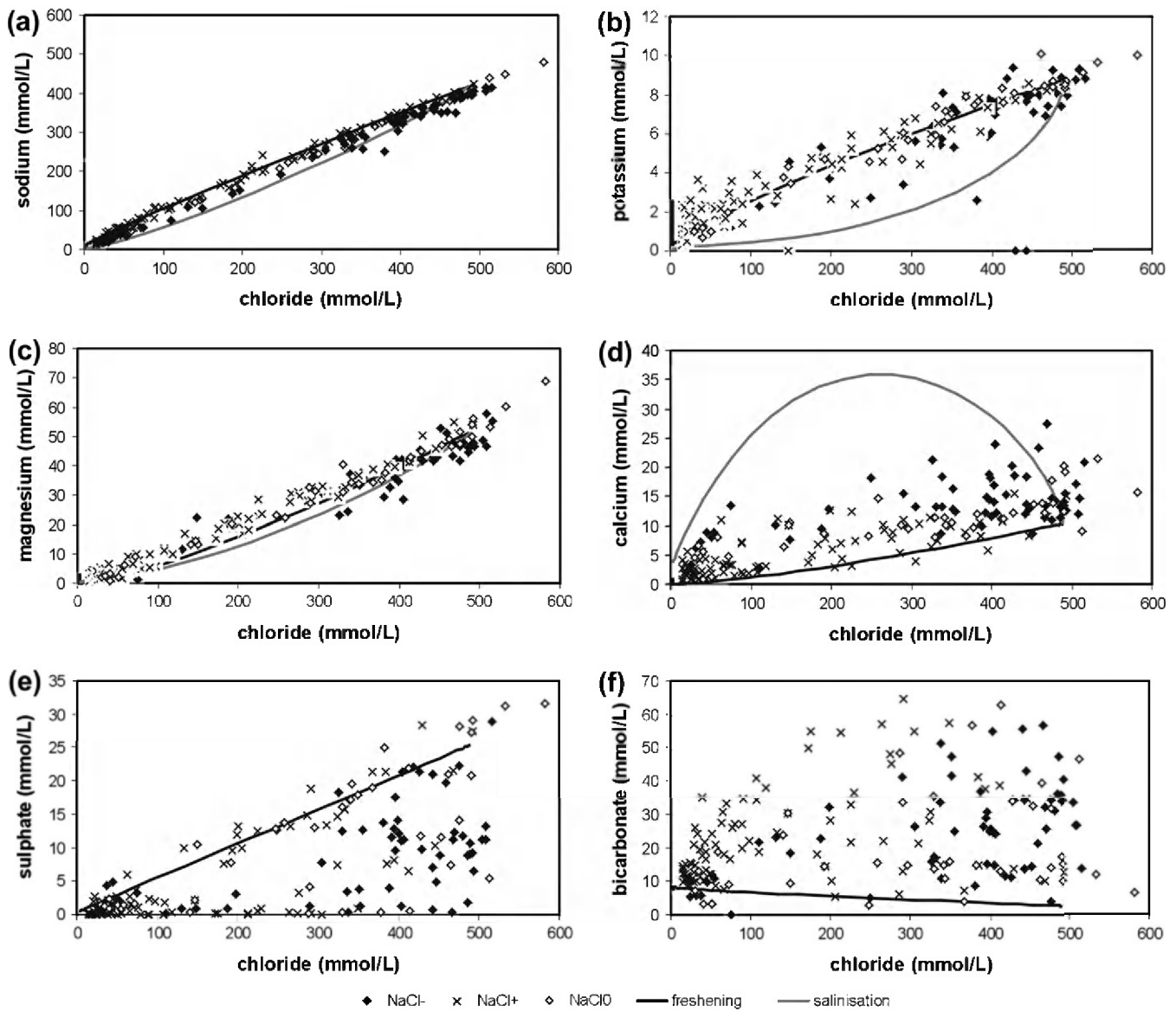
Fig. 10. Na^+, K^+, Ca^{2+}, Mg^{2+}, SO_4^{2-} and HCO_3^- as function of Cl^- for the NaCl subtype of the relict Holocene hydrosome. Concentrations for the freshening and salinisation experiment calculated with PHREEQC are also indicated.

versus Cl^- concentration for the freshening modeling calculated with PHREEQC are also plotted on these figures. Additionally, a salinisation modeling was calculated, whereby freshwater (CaH-CO₃0 subtype, Table 2) is replaced by North Sea water and the resulting concentrations versus Cl^- concentration are plotted on Fig. 10. Results of the salinisation modeling are also given in Fig. 8b, are plotted on the Piper diagram (Fig. 5) and the relative percentages are given in Fig. 6b and d. The salinisation modeling shows a typical sequence of water types which should result in corresponding hydrochemical facies in the aquifer. The CaHCO₃0 evolves first in $CaHCO_3^-$, the BEX illustrating the salinisation. Subsequently, $CaMix^-$ and $CaCl^-$ are found and finally, $NaCl^-$ and NaCl0 develop. The $CaMix^-$, $CaCl^-$ and $NaCl^-$ are typically found in the mixing zone.

Bicarbonate and SO_4^{2-} concentrations versus Cl^- concentrations show the same evolution for the freshening as for the salinisation modeling and only the former is plotted (Fig. 9). In the freshening calculation, all species show conservative behavior for the relatively large Cl^- concentrations encountered in the NaCl subtype and plot on a straight line between the seawater and the fresh replacement water. Consequently, mixing in the transition zone

between fresh and saltwater is the dominant process determining the resulting groundwater composition. In the salinisation calculation, HCO_3^- and SO_4^{2-} show perfect conservative behavior, only influenced by mixing. Magnesium evolution is almost according to a conservative mixing line, whereas the other species clearly show non-conservative behavior. Sodium, K^+ and to a lesser extent Mg^{2+} are depleted during the salinisation whereas Ca^{2+} is enriched. Sodium, K^+ and Mg^{2+} present in the displacing saltwater are thereby exchanged for Ca^{2+} present on the exchanger.

How does the data set compare to the freshening and salinisation calculations? Concerning Na^+, the NaCl+ subtype has a slightly greater Na^+ concentration than the $NaCl^-$ subtype of a comparable Cl^- concentration. Samples with a positive BEX, indicating freshening, plot close to the freshening calculations, whereas samples with a negative BEX, indicating salinisation, plot close to the salinisation calculation. This is not the case for K^+, where there is a relatively large spread around the freshening line. More or less the same applies for Mg^{2+} where the samples are scattered around the freshening and salinisation line. Calcium shows the most striking difference between the freshening and salinisation modeling. Most of the samples plot between these two lines. In general, samples

with a positive BEX plot closer to the freshening line, whereas samples with a negative BEX plot closer to the salinisation line. Consequently, water samples from the RHH seem to indicate that both freshening and salinisation has occurred in the RHH. Note also that the NaCl subtype plots in the Piper plot along the freshening line as well as along the salinisation line.

Indication of both freshening and salinising behavior is very well illustrated by the relative Na^+ percentage (Fig. 6a and b). The PHREEQC calculations show an initial increase of the Na^+ percentage during freshening due to exchange of Na^+ for Ca^{2+}. During the final stages of the freshening, Na^+ is exhausted on the exchanger and the percentage decreases. Salinisation shows an increase of the Na^+ percentage which is completely different from the decrease during freshening. The Na^+ percentages of the actual samples plot between the calculated freshening and salinisation line. This is not only indicating freshening as well as salinisation evidence in the RHH but also a more complex evolution. Instead of starting from the end members (seawater or fresh $CaHCO_3 0$) brackish water $CaHCO_3$ or NaCl, $NaHCO_3$ or $MgHCO_3$ subtypes could for instance become fresher or more saline because of the hydrogeological evolution.

The Ca/Cl, $(Ca + Mg)/Cl$ and Mg/Ca molar ratios are, together with the BEX, strong indicators for freshening or salinisation in aquifers (Jones et al., 1999). These ratios are given for the NaCl and CaCl subtypes in Table 3. A Cl/Na molar ratio of 1.16 is typical for seawater. Brackish and salt $NaCl^-$ subtypes have a relatively large Cl/Na ratios reflecting salinisation, its lower limit being in the order of the seawater ratio of 1.16. Brackish and salt $NaCl^+$ subtypes have a lower ratio in line with the positive BEX indicating freshening in the samples. Salt $NaCl^+$ subtypes have a ratio in the order of the seawater ratio whereas the brackish samples have a distinctly lower ratio. Samples with a neutral BEX have Cl/Na ratios between those found in samples with a positive or negative BEX. The Ca–Cl samples have a relatively high Cl/Na ratio, especially those with a negative BEX, reflecting salinisation. The $(Ca + Mg)/Cl$ molar ratios show a somewhat different pattern. Salt samples (with either positive, negative or neutral BEX) show the same ratio, between 0.10 to 0.16. The same applies for the brackish samples for which the ratio is between 0.10 and 0.37. Note that the lower limit of the $(Ca + Mg)/Cl$ ratio is the same for brackish and salt samples. The CaCl subtype shows somewhat higher ratios. The fact that there is no clear freshening or salinisation signal in the $(Ca + Mg)/Cl$ as in the Cl/Na is due to dissolution of carbonate minerals which influences, besides the cation exchange, the Ca^{2+} concentration. The Cl/Na ratio is mainly determined by cation exchange. The Mg/Ca molar ratio also reflects carbonate dissolution. The Mg/Ca of seawater is normally between 4.5 and 5.2. Most NaCl subtypes have a much lower ratio indicating an increase of Ca^{2+} with respect to conservative mixing of seawater and freshwater. The SI of calcite for NaCl samples is between -0.5 and 1.0 indicating equilibrium or slightly supersaturated conditions.

Stuyfzand and Stuurman (2008) identified two types of brackish and salt relict Holocene transgression waters for the Netherlands. Since the situation is comparable in the Belgian coastal plain, these

also apply. The first is an open marine estuarine or tidal gully type. It is formed in high energy areas open to the sea, with a sandy floor limiting contact with clay and peat. This results in water quality with relatively low alkalinity (5–10 mmol/L HCO_3^-). The second type is the lagoonal type which must have infiltrated in low energy areas protected from direct incursions by the sea, allowing abundant contact with clay and peat. This results in higher alkalinity (10–65 mol/L HCO_3^-) which combines with extremes in SO_4 reduction due to the oxidation of organic matter. Fig. 10 shows HCO_3^- as a function of Cl^- for the NaCl subtypes and this shows a wide range of HCO_3^- concentrations (up to 65 mmol/L) for all Cl^- concentrations. For many samples, SO_4^{2-} concentrations are significantly lower than the mixing line. Consequently, most samples in the data set have high HCO_3^- concentrations and are characterized by SO_4 reduction, pointing to the lagoonal type predominating in the dataset. This is in agreement with the fresh and brackish water marshes which were present between 5500 and 3400 BP, the high organic matter content of the sediments and the occurrence of significant peat layers in large parts of the area. Distinction between the open marine estuarine or tidal gully type and lagoonal type could be made based on the SO_4^{2-} concentration. Samples which plot close to the mixing line in Fig. 10 are of the former type, samples which show lower concentrations are of the latter type. As indicated by Stuyfzand and Stuurman (2008), CH_4, increased nutrient concentrations and Cl/Br ratios are further indicators for the lagoonal type. Only NH_4^+ concentrations are available in the present dataset and these increase with increasing HCO_3^- concentrations. For HCO_3^- concentration below 10 mmol/L, NH_4^+ concentrations are less than 0.7 mmol/L. For HCO_3^- concentrations of 60 mmol/L, NH_4^+ concentrations increase and range between 2.5 and 4 mmol/L.

4.5. Groundwater ages

Sparse age determinations are available for coastal groundwater but they are of interest. De Breuck and De Moor (1974) give radiocarbon dates of a RHH water sample taken below the Houtave creek ridge. It is a $S4NaCl^-$ type and its ^{14}C age is 4000 ± 180 a. Devos (1984) gives 5 ^{14}C ages, all of the samples from the the RHH. Two samples are of the $B4NaCl^+$ type and have ages of 1375 ± 95 and 2545 ± 150 a. A B4 $NaCl^-$ type is dated as 1975 ± 210 a. The oldest samples are a $b2NaCl0$ type (8055 ± 75 a) and a $B5NaHCO_3^+$ sample having an age of 8370 ± 105 a. Sampling was carried out in the field using the IAEA procedure (Tamers and Scharpensel, 1970). Total Inorganic C (TIC) was precipitated as $BaCO_3$ and these precipitates were analysed at the Institut Royal du Patrimoine Artistique (IRPA) at Brussels (De Breuck and De Moor, 1974) and in the Niedersächsisches Landesamt für Bodenforschung at Hannover (Devos, 1984). The $BaCO_3$ precipitate was converted to CO_2 by acidification and subsequently to CH_4 that is used for the ^{14}C analysis using a proportional gas counter, the ^{13}C being measured with a mass spectrometer. The ^{14}C dating model of Münnich (1957) was used by Devos (1984) whereas De Breuck and De Moor (1974) give conventional ^{14}C ages.

Vandenbohede et al. (2011) gives ages of 4 samples taken in the freshwater lens south of Oostende using $^3H/^3He$. The sampling for the $^3H/^3He$ analysis and groundwater dating was performed with a new technique for sampling of noble gases that employs diffusion samplers developed by the University of Utah (Gardner and Solomon, 2009). Samples for ^3H and Cl^- analyses were also collected. The diffusion samples and the ^3H samples were both analysed by mass spectrometry. The ^3H content was measured by the He ingrowth method, where the water sample is degassed, sealed and left to sit for 6–12 weeks while ^3H decays to ^3He, which is then determined. All these samples show young ages (<40 a).

These groundwater ages illustrate the pre-impoldering age of the RHH while the wide range of dates in the RHH indicates the

Table 3
Cl/Na and (Ca + Mg)/Cl molar ratios for the CaCl and NaCl subtypes.

	Cl/Na	(Ca + Mg)/Cl	Mg/Ca
$CaCl^-$	1.3–4.5	0.20–0.57	0.17–0.36
$CaCl^+$	1.14–1.48	0.45–0.56	0.34–0.44
$(B-b)NaCl^-$	1.15–1.60	0.10–0.30	0.8–3.8
$SNaCl^-$	1.10–1.35	0.10–0.16	1.81–4.00
$(B-b)NaCl^+$	0.64–1.10	0.09–0.37	0.39–5.31
$SNaCl^+$	1.10–1.16	0.11–0.15	1.19–6.95
$(B-b)NaCl0$	1.08–1.30	0.11–0.26	0.36–4.11
$SNaCl0$	1.14–1.27	0.11–0.15	2.67–5.03

Holocene evolution which is reflected in the pore water composition. The groundwater ages in a freshwater lens illustrate the young ages of the pore water. Pore water in the fresh water lenses is consequently very recently infiltrated rain water.

4.6. Concentration ranges

Even within a given subtype, concentrations of a given species can show a relatively large range. This is evident from Table 2, the Piper plot (Fig. 5) and the relative percentages (Fig. 6). In this section, the underlying reasons are discussed. As explained in the previous section, the water quality observed in the RHH is not necessarily the product of one clearly defined phase of freshening or salinisation but could be due to subsequent phases of freshening and salinisation, consequently, it is not necessarily the case that one of the end products (saline NaCl0 or fresh CaHCO30) is the displaced water type. The effect of this on the water quality is shown in Fig. 11a and b. These figures show the previously discussed water quality evolution when fresh recharge water displaces seawater or vice versa, which were calculated with the PHREEQC column modeling run. Fig. 11a shows water quality evolution if a CaMix, CaCl or a brackish NaCl subtype is replaced by freshwater. This is a situation which could have occurred during the general late-Holocene freshening of the aquifer or during freshening periods (for instance because of the evolution of a freshwater marsh) during earlier periods. Starting from a brackish NaCl⁻ subtype, the freshening line shows the same general evolution as when starting from pure seawater. However, the intermediate water contains relatively more Ca^{2+} and Mg^{2+} and relatively less Na^+ and K^+. Consequently, this partly explains the spread of concentrations in the NaCl and NaHCO₃ subtypes. Starting from a CaCl subtype, evolution through a CaMix to the CaHCO₃ end subtype is seen. This explains the positive as well as negative BEX which can be observed in the CaCl, CaMix and CaHCO₃ subtypes. Replacing a fresh CaMix⁻ subtype with freshwater results fairly quickly in a CaHCO₃0 subtype. Fig. 11b shows the opposite, whereby the evolution of salinisation is calculated starting from different subtypes (brackish NaCl, NaHCO₃ and MgHCO₃). This is a situation which could have occurred for different scenarios during the Holocene

transgression (lateral migration of tidal gullies to a fresh environment, inundation of brackish or freshwater marshes). Displacing these water types with seawater shows the same evolution as displacing freshwater. However, the intermediate waters contain relatively less Ca^{2+} and Mg^{2+} and relatively more Na^+ and K^+. Subsequently, it also partly explains the spread of concentrations in the NaCl and NaHCO₃ subtypes and in Fig. 11a the occurrence of positive as well as negative BEX for the NaCl subtype. Starting from a MgHCO3 subtype, salinisation leads to $MgCl^+$ subtypes before evolving to NaCl subtypes.

A further influence on the concentration range is the variation in cation exchange capacity (CEC). The freshening and salinisation modeling is performed with a CEC of 6 mmol/kg but because of variation in clay and organic matter content, CEC will also vary (Appelo and Postma, 2005). A last important factor explaining the spreading of subtypes on the Piper plot is the SO_4^{2-} concentration, especially for the CaHCO₃ subtype. As is shown in Fig. 9a, SO_4^{2-} concentration has a large range in the CaHCO₃ subtype because of different concentrations in the recharge water (due to pyrite oxidation and/or agricultural contamination) and the degree of SO₄ reduction.

5. Conclusions

In the central Belgian coastal plain, three hydrosomes could be distinguished: the dune hydrosome (DH), polder hydrosome (PH) and relict Holocene hydrosome (RHH). These hydrosomes originated during the Holocene evolution of the coastal plain. The RHH containing brackish to saltwater, is found in the deeper part of the Quaternary phreatic aquifer, and dates from before land reclamation (impoldering) which started from about the 10th century AD. The PH and DH containing freshwater, are found in the upper part of the Quaternary phreatic aquifer, and date from during and after the impoldering.

Quaternary geological evolution was dominated by a continued transgression of the sea and progressive silting up of the coastal plain. Between 7500 and 5500 BP large parts were no longer inundated by the sea because of a decrease in the rate of sea level rise. A mud-flat environment with mud and salt-marshes developed and
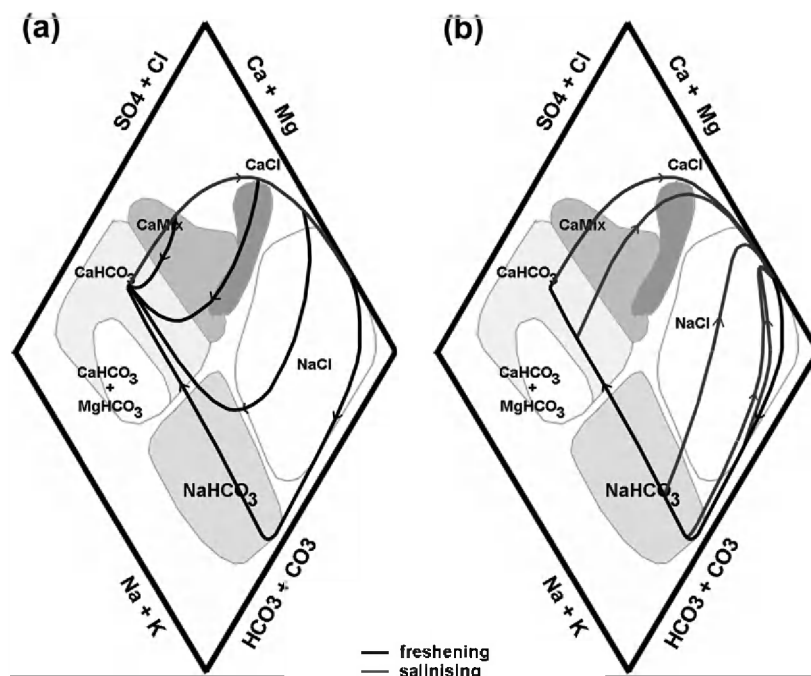

Fig. 11. Left figure (a) shows a Piper plot with freshening evolution starting from different subtypes whereas (b) shows salinisation evolution starting from different subtypes.

was incised by tidal channels and gullies development. At some locations, salt marshes evolved into freshwater marshes with reed vegetation. The aquifer was recharged by mainly salt and brackish water and brackish and salt NaCl subtypes would have dominated the aquifer. Additionally, freshening of the aquifer will have occurred in the freshwater marshes and higher parts of the coastal plain. The highly dynamic nature of the tidally dominated system means that saline conditions could evolve into freshening conditions and vice versa. For instance, lateral migration of gullies into a freshwater marsh environment would lead to a transitioning from freshening to saline conditions and mixing of fresh and saltwater. From about 5500 BP, many parts of the coastal plain were no longer under the constant influence of the sea and became only inundated temporally during major storm events, enhancing the freshening of the aquifer. This ended with a renewed invasion of the sea from about 3400 BP, leading to a phase of general salinisation of the aquifer. Consequently, a range number of water types is expected to be found in the RHH because of this complex evolution of different episodes of salinisation and freshening of the aquifer. Consequently, because of the dynamic environments that groundwater originated from, it is almost impossible to delineate spatially or map, different hydrochemical facies within the RHH. The most important water types are brackish and salt NaCl subtypes with both positive and negative BEX, illustrating mixing of fresh and saltwater and both freshening and salinisation of the groundwater. However, brackish $NaHCO_3$, brackish CaCl, NaMix and CaMix exist, pointing to freshening as well as to salinisation of the groundwaters.

Because of the impoldering, the North Sea could no longer inundate the coastal plain and freshwater could recharge the aquifer. Whereas the period preceding the impoldering is characterized by locally (fast) changing alternation between freshening and salinisation, the period after impoldering is generally characterized by a freshening of the aquifer. The older brackish and saline groundwater is replaced by fresh recharge water, leading to the formation of freshwater lenses. The PH and the DH differ mainly by location, the former is found in the polder and the latter in the dunes. Along a streamline (for instance in a freshwater lens) the following water subtypes (and hydrochemical facies) can be distinguished: $CaHCO_30$, $CaHCO_3^+$, $MgHCO_3^+$, and $NaHCO_3^-$. This sequence mainly reflects cation exchange whereby Ca^{2+} exchanges first for Na^+ (and K^+) and then for Mg^{2+} (and K^+). Increases in HCO_3^- and Ca^{2+} concentrations with respect to pure mixing of seawater and fresh recharge water identifies carbonate mineral (calcite) dissolution as a second important reaction. Reduction of organic material is a third mechanism determining the overall chemical composition of the samples. Because of denitrification, NO_3^- concentrations are in general very low, concentrations are all, but for a few exceptions, well below the European limit of 50 mg/L. Oxidation of pyrite in the upper part of the aquifer, followed by SO_4 reduction deeper in the aquifer results in a wide range of SO_4^{2-} concentrations. In some cases SO_4^{2-} concentrations can be high enough to be reflected in the water type leading to (F-f)(2–4)CaMix or even (F-f)4CaSO$_4^+$. The latter is almost certainly due to agricultural contamination.

Acknowledgements

References

Ampe, C., 1999. Research of the Dune Soils of the Flemisch and Northern French Coast with Special Attention to Ecosystem Dynamics and Nature Preservation. Ph.D. Dissertation, Ghent Univ. (in Dutch).

Andersen, M.S., Jakobsen, V.N.R., Postma, D., 2005. Geochemical processes and solute transport at the seawater/freshwater interface of a sandy aquifer. Geochim. Cosmochim. Acta 69, 3979–3994.

Appelo, C.A.J., Postma, D., 2005. Geochemistry Groundwater and Pollution, second ed. A.A. Balkema.

Back, W., 1960. Origin of Hydrochemical Facies of Ground Water in the Atlantic Coastal Plain. 21st Internat. Geol. Cong., Copenhagen 1960, Rep. pt. 1, pp. 87–95.

Baeteman, C., 1985. Development and evolution of sedimentary environments during the Holocene in the western coastal plain of Belgium. Eiszeitalter Gegenwart 35, 23–32.

Baeteman, C., 1999. The Holocene depositional history of the IJzer palaeovalley (western Belgian coastal plain) with reference to the factors controlling the formation of intercalated peat beds. Geol. Belg. 2 (3–4), 39–72.

Baeteman, C., Beets, D.J., Van Strydonck, M., 1999. Tidal crevasse splays as the cause of rapid changes in the rate of aggradation in the Holocene tidal deposits of the Belgian Coastal Plain. Quatern. Int. 56, 3–13.

Barlow, P.M., Reichard, E.G., 2010. Saltwater intrusion in coastal regions of North America. Hydrogeol. J. 18, 247–260.

Beekman, H.E., 1991. Ion Chromatography of Fresh and Salt Water Intrusion. Ph.D. Dissertation, Vrije Univ., Amsterdam.

Calvache, M.L., Pulido-Bosch, A., 1997. Effects of geology and human activity on the dynamics of salt-water intrusion in three coastal aquifers in southern Spain. Environ. Geol. 30, 215–223.

Capaccioni, B., Didero, M., Paletta, C., Didero, L., 2005. Saline intrusion and refreshening in a multilayer coastal aquifer in the Catania Plain (Sicily, Southern Italy): dynamics of degradation processes according to the hydrochemical characteristics of groundwaters. J. Hydrol. 307, 1–16.

Coleman, J.M., 1981. Deltas: Processes of Deposition and Models for Exploration. Internat. Human Resour; Dev. Corp., Boston, Mass.

Costudio, E., 1997. Studying, monitoring and controlling seawater intrusion in coastal aquifers. In: Guidelines for Study, Monitoring and Control, FAO Water Reports No. 11, pp. 7–23.

Custodio, E., 2010. Coastal aquifers of Europe: an overview. Hydrogeol. J. 18, 269–280.

De Breuck, W., De Moor, G., 1972. The salinisation of the Quaternary sediments in the coastal area of Belgium. In: Proc. 3rd Salt Water Intrusion Meeting, Copenhagen, 1972, pp. 6–19.

De Breuck, W., De Moor, G., 1974. The evolution of the coastal aquifer of Belgium. In: Proc. 4th Salt Water Intrusion Meeting, Ghent, 1974, pp. 158–172.

De Breuck, W., De Moor, G., Tavernier, R., 1974. Depth of the fresh–salt water interface in the unconfined aquifer of the Belgian coastal area (1963–1973). In: Proc. 4th Salt Water Intrusion Meeting, Gent, Annex-map, Scale 1/10,0000.

De Leenheer, L., Van Ruymbeke, M., 1960. Monograph of the Sea Polders: Repertory of the Pedogogical Characteristics of the Main Soil Types in the Belgian Sea Polders. Pedologie – Verhandelingen van de Belgische Bodemkundige Vereniging, 2 (in Dutch).

de Louw, P.G.B., Oude Essink, G.H.P., Stuyfzand, P.J., van der Zee, S.E.A.T.M., 2010. Upward groundwater flow in boils as the dominant mechanism of salinisation in deep polders, The Netherlands. J. Hydrol. 394, 494–506.

De Vries, J.J., 1981. Fresh and salt groundwater in the Dutch coastal area in relation to geomorphological evolution. Geol. Mijnbouw 60, 363–368.

Devos, J., 1984. Hydrogeology of the Dune Area East of De Haan. Ph.D. Dissertation, Ghent Univ. (in Dutch).

El Yaouti, F., El Mandour, A., Khattach, D., Benavente, J., Kaufmann, O., 2009. Salinization processes in the unconfined aquifer of Bou-Areg (NE Morocco): a geostatistical, geochemical, and tomographic study. Appl. Geochem. 24, 16–31.

Ervynck, A., Baeteman, C., Demiddele, H., Hollevoet, Y., Pieters, M., Schelvis, J., Tys, D., Van Strydonck, M., Verhaeghe, F., 1999. Human occupation because of regression, or the cause of a transgression? A critical review of the interaction between geological events and human occupation in the Belgian coastal plain during the first millennium AD. Probleme der Küstenforschung im südlichen Nordseegebiet 26, pp. 97–121.

Franceschi, G., 1975. Geological Study of the Shallow Layers at Houtave. M.Sc. Dissertation, Ghent University (in Dutch).

Gardner, P., Solomon, D.K., 2009. An advanced passive diffusion sampler for the determination of dissolved gas concentrations. Water Resour. Res. 45, W06423.

Giménez, E., Morell, I., 1997. Hydrogeochemical analysis of salinization processes in the coastal aquifer of Oropesa (Castellon, Spain). Environ. Geol. 29, 118–131.

Giménez-Forcada, E., Bencini, A., Pranzini, G., 2010. Hydrogeochemical considerations about the origin of groundwater salinization in some coastal plains of Elba Island (Tuscany, Italy). Environ. Geochem. Health 32, 243–257.

Grube, A., Wichmann, K., Hahn, J., Nachtigall, K.H., 2000. Geogene Grundwasserversalzung in den Poren-Grundwasserleitern Norddeutschlands und ihre Bedeutung für die Wasserwirtschaft. DVGW-Technologiezentrum Wasser Karlsruhe, Band 9, Karlsruhe.

Jones, B.F., Vengosh, A., Rosenthal, E., Yechieli, Y., 1999. Geochemical investigations. In: Bear, J., Cheng, A.H.-D., Ouazar, D., Herrera, I. (Eds.), Seawater Intrusion in

Coastal Aquifer – Concepts, Methods and Practices. Theory and Applications of Transport in Porous Media, vol. 14, pp. 51–72.

Lebbe, L., Vandenbohede, A., Waeyaert., P., 2006. Refinement of the HCOV Mapping of the Coast and Polder System and Application of it in a Local Axial Symmetric Model in the Support of Advice for Groundwater Extractions in the Salinated Phreatic Aquifer. Scientific Report, Ghent University (in Dutch).

Münnich, K.O., 1957. Messungen des 14C-Gehaltes von hartem Grundwasser. Naturwissenschaften 55, 158–163.

Oude Essink, G.H.P., 2001. Salt water intrusion in a three-dimensional groundwater system in the netherlands: a numerical study. Transp Porous Media 43, 137–158.

Oude Essink, G.H.P., van Baaren, E.S., de Louw, P.G.B., 2010. Effects of climate change on coastal groundwater systems: a modeling study in the Netherlands. Water Resour. Res. 46, W00F04.

Parkhurst, D.L., Appelo, C.A.J., 1999. User's Guide to PHREEQC (Version 2): a Computer Program for Speciation, Batch-Reaction, One-dimensional Transport, and Inverse Geochemical Calculations. US Geol. Surv. Water-Resour. Invest. Rep. 99-4259.

Post, V.E.A., Van der Plicht, H., Meijer, H.A.J., 2003. The origin of brackish and saline groundwater in the coastal area of the Netherlands. Netherlands J. Geosci. – Geol. Mijnbouw 82 (2), 133–147.

Pulido-Leboeuf, P., 2004. Seawater intrusion and associated processes in a small coastal complex aquifer (Castell de Ferro, Spain). Appl. Geochem. 19, 1517–1527.

Rusak, A., Sivan, O., 2010. Hydrogeochemical tool to identify salinisation or freshening of coastal aquifers determined from combined field work, experiments, and modeling. Environ. Sci. Technol. 44, 4096–4102.

Sivan, O., Yechieli, Y., Herut, B., Lazar, B., 2005. Geochemical evolution and timescale of seawater intrusion into the coastal aquifer of Israel. Geochim. Cosmochim. Acta 69, 579–592.

Stamatis, G., Voudouris, K., 2003. Marine and human activity influences on the groundwater quality of southern Korinthos area (Greece). Hydrol. Process. 17, 2327–2345.

Stufzand, P.J., 1991. A new hydrochemical classification of water types: principles and application to the coastal-dunes aquifer of the Netherlands. In: De Breuck, W. (Ed.), Hydrogeology of Salt Water Intrusion: A Selection of SWIM Papers. IAH International Contributions to Hydrogeology, vol. 11, pp. 329–343.

Stuyfzand, P.J., 1989. A new hydrochemical classification of watertypes. IAHS Publ. 182, 89–98.

Stuyfzand, P.J., 1993a. Hydrochemistry and Hydrology of the Coastal Dune Area of the Western Netherlands. Ph.D. Thesis, Nieuwegein, KIWA, Afd. Onderzoek & Advies.

Stuyfzand, P.J., 1993b. Behaviour of major and tracé constituents in fresh and salt water intrusion, in the western Netherlands. In: Proc. 12th Salt Water Intrusion Meeting, Barcelona 1992, pp. 143–160.

Stuyfzand, P.J., 1999. Patterns in ground water chemistry resulting from ground water flow. Hydrogeol. J. 7, 15–27.

Stuyfzand, P.J., 2008. Base exchange indices as indicators of salinization or freshening of (coastal) aquifers. In: Proc. 20th Salt Water Intrusion Meeting, June 23–27 2008, Naples (Fl) USA, Univ. Florida, IFAS Research, pp. 262–265.

Stuyfzand, P.J., Stuurman, R.J., 1994. Recognition and genesis of various brackish to hypersaline groundwaters in The Netherlands. In: Proc. 13th Salt Water Intrusion Meeting, June 1994, Cagliari Italy, Univ. Cagliari, Fac. Engineering, pp. 125–136.

Stuyfzand, P.J., Stuurman, R.J., 2008. Origin, distribution and chemical mass balances of non-anthropogenic, brackish and (hyper)saline groundwaters in the Netherlands. In: Proc. 1st SWIM-SWICA Joint Saltwater Intrusion Conference, Cagliari, Italy, 2006, pp. 151–164.

Tamers, M.A., Scharpensel, H.W., 1970. Sequential Sampling of Radiocarbon in Groundwater. Isotope Hydrology. IAEA, Vienna, pp. 241–256.

van Dam, J., 1999. Exploitation, restoration and management. In: Bear, J., Cheng, A.H.-D., Ouazar, D., Herrera, I. (Eds.), Seawater Intrusion in Coastal Aquifer – Concepts, Methods and Practices. Theory and Applications of Transport in Porous Media, vol. 14, pp. 73–125.

Vandenbohede, A., Lebbe, L., 2002. Numerical modelling and hydrochemical characterisation of a fresh water lens in the Belgian coastal plain. Hydrogeol. J. 10, 576–586.

Vandenbohede, A., Van Houtte, E., Lebbe, L., 2009. Water quality changes in the dunes of the western Belgian coastal plain due to artificial recharge of tertiary treated wastewater. Appl. Geochem. 24, 370–382.

Vandenbohede, A., Courtens, C., Lebbe, L., De Breuck, W., 2010. Fresh–salt water distribution in the central Belgian coastal plain: an update. Geol. Belg. 11 (3), 163–172.

Vandenbohede, A., Hinsby, K., Courtens, C., Lebbe, L., 2011. Flow and transport model of a polder area in the Belgian coastal plain: example of data integration. Hydrogeol. J. doi:10.1007/s10040-011-0781-7.

Wiederhold, H., Siemon, B., Steuer, A., Schaumann, G., Meyer, U., Binot, F., Kühne, K., 2010. Coastal aquifers and saltwater intrusions in focus of airborne electromagnetic surveys in Northern Germany. In: Proc. 21st Salt Water Intrusion Meeting, Azores, pp. 94–97.